

Unidirectional electric field enables reversible ferroelectric domain engineering

Received: 22 April 2025

Accepted: 7 August 2025

Published online: 15 August 2025

Check for updates

Xingan Jiang¹, Muzhi Li², Yuanyuan Cui³, Xiao Wu⁴, Zunyi Deng³,
Xiangping Zhang^{3,5}, Jianming Deng⁶, Xiaolei Wang⁷, Dongdong Zhang¹,
Xiangdong Yang¹, Zhuoyin Peng², Zhao Liang¹✉, Xueyun Wang³✉ &
Weiyu Yang¹✉

The deterministic control of ferroelectric polarization via an external field is critical for advancing the technologies of modern information storage. Conventionally, reversible and cyclic polarization switching in ferroelectric materials requires bipolar electric fields. The present work demonstrates the efficient reversible and cyclic ferroelectric domain switching under a unipolar electric field in van der Waals ferroelectric CuInP_2S_6 , enabled by Cu-ion migration across van der Waals gaps. It further unveils the remarkable “shape memory” effect of manipulated domains, and the programmable domain patterning under a unipolar electric field. These findings not only deepen the understanding of ferro-ionic coupling mechanism, but also provide insights into the origin of multiple polarization states, negative capacitance, and the quantized charge transport, paving the way for emerging storage technologies and low-power neuromorphic applications.

Ferroelectric materials possess a switchable spontaneous polarization, which attracts a diverse portfolio of applications, such as memory devices^{1–3}, sensors^{4–6}, and low-power electronic devices^{7–9}. Van der Waals (vdW) ferroelectrics have attracted significant interest due to their unique attributes, such as atomically thin layers with dangling-bond-free surfaces and weak interlayer interactions^{10,11}. These features enable ferroelectricity to be realized at the atomic scale^{12–15}, and facilitate vdW integration with diverse substrates as well as the construction of vdW heterojunctions without lattice limitation and interfacial damage¹⁶, which paves the way for wafer-scale fabrication of high-performance 2D/3D device architectures^{17,18}.

The ferroelectric polarization is a fundamental order parameter that responds to external electric fields^{10,11}. The deterministic control of polarization switching with an external electric field is essential for emerging functionalities¹⁹. Traditional ferroelectric materials feature displacive ions confined in the lattice, giving rise to a double-well

energy landscape. In such case, the polarization aligns along the identical direction to the external electric field, implying that the reversible polarization switching must require two opposite (\pm) electric fields²⁰. However, this scenario might be circumvented by taking highly mobile ions into account^{21–23}, exemplified by the vdW ferroionic CuInP_2S_6 (CIPS). Since Belianinov et al.²⁴ and Liu et al.²⁵ reported the room-temperature switchable ferroelectricity of CIPS nanoflakes, this material system has rapidly inspired significant interest. Subsequent studies extensively investigate the Cu ion migration dynamics, which reveals that the ferro-ionic coupling behavior offers rich energy landscapes including quadruple-well and sextuple-well configurations, enabling the multiple polarization states control and negative capacitance^{21,26,27}. Recently, Vanderbilt et al.²⁸ theoretically proposed the scenario of quantized charge transport–polarization evolving by a quantum as the mobile Cu ions shift to neighboring layer, delivering great potential for low-power

¹Institute of Micro/Nano Materials and Devices, Ningbo University of Technology, Ningbo City, China. ²School of Energy and Power Engineering, Changsha University of Science & Technology, Changsha, China. ³School of Aerospace Engineering, Beijing Institute of Technology, Beijing, China. ⁴College of Materials Science and Engineering, Fuzhou University, Fuzhou, China. ⁵Department of Materials Science and Engineering, Southern University of Science and Technology, Shenzhen, Guangdong, China. ⁶Guangdong Provincial Key Laboratory of Electronic Functional Materials and Devices, Huizhou University, Huizhou, Guangdong, China. ⁷School of Physics and Optoelectronic Engineering, Beijing University of Technology, Beijing, China. ✉e-mail: walleliang@hnu.edu.cn; xueyun@bit.edu.cn; weiyuyang@tsinghua.org.cn

neuromorphic applications^{29,30}. Yet, the experimental realization of cyclic ferroelectric domain control in such systems, as a critical piece of evidence, has remained elusive. Moreover, the material damage is recognized as the primary obstacle in CIPS for ferroelectric domain control using the tip-based methodology^{31,32}. As the conductive substrate (e.g., Au/SiO₂/Si) is utilized and a bias voltage is applied to the conductive substrate, the tip-concentrated current induces significant surface protrusions, substantially preventing the ferroelectric domain manipulation^{31,32}.

Herein, we report the reversible ferroelectric domain engineering enabled by unipolar electric fields, which is fundamentally distinct from conventional bipolar ($\pm V$) field control. An insulating SiO₂/Si substrate is utilized while the bias voltage is applied through the tip, establishing an electrically open-circuit condition to prevent current generation. This refined technique substantially mitigates the CIPS material damage and permits the repeated bias-application and large-area domain engineering. Accordingly, it enables the achievement of visualizing the cyclic ferroelectric domain control, the domain shape

memory effect, and programmable domain patterning, facilely by a unidirectional electric field. Our findings provide evidence for ferroelectric domain control in long-displacement ferroelectrics, which is fundamentally important for developing memory and neuromorphic computing devices based on ferroelectric domain engineering in a similar ferro-ionic coupling system.

Results

Cyclic domain switching under a unidirectional electric field

Figure 1a illustrates the layered structure of CuInP₂S₆ (CIPS) with vdW gaps. Two distinct Cu ions sites are identified near the upper and lower sulfur atoms, giving rise to two states with upward ($P \uparrow$, \odot) and downward ($P \downarrow$, \otimes) polarizations, respectively³¹. Under electric field, the Cu ions can undergo long-range migration, holding significant promise for memristor-based neuromorphic applications^{33–36}. Herein, we focus on the ferroelectric domain manipulation in CIPS. Figure 1b shows the measurement setup to manipulate the ferroelectric domain, where the conductive substrate (Au/SiO₂/Si) is utilized and bias voltage

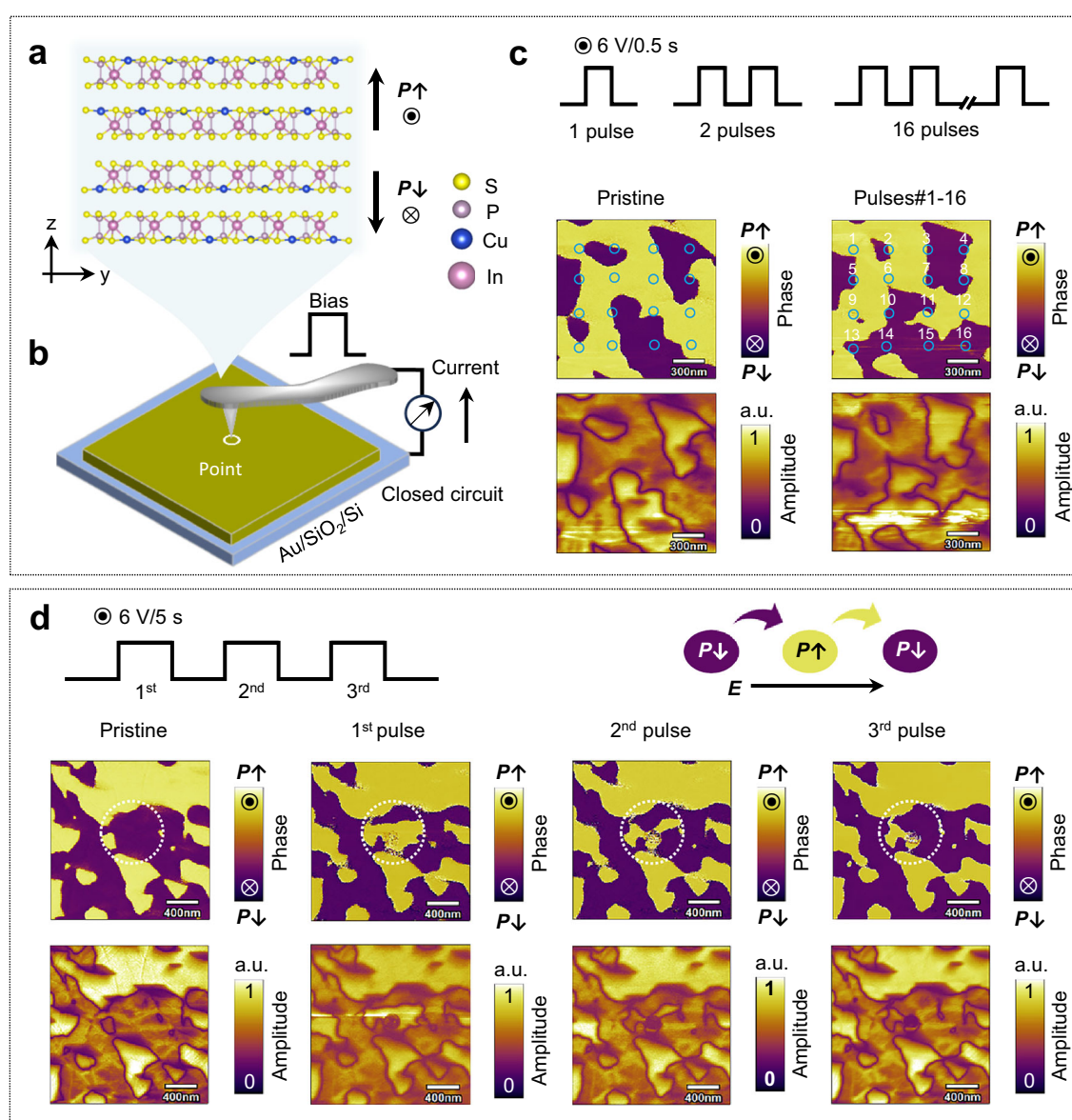


Fig. 1 | Reversible and cyclic domain switching under unidirectional electric fields. **a** Crystalline structure with two Cu sites in the sulfur octahedron, showing the opposite polarization. **b** Diagram of short-duration pulse bias applied at a central location via conductive tip in a closed circuit. **c** Ferroelectric domain

switching with increased numbers of bias pulses (6 V, 0.5 s) at 16 different locations. **d** Ferroelectric domain switching by 3 sets of bias pulses (6 V, 0.5 s) at a fixed location. The white dashed circle indicates the region influenced by the tip electric field.

is applied to the conductive substrate. Accordingly, a series of pulse biases (6 V for 0.5 s) are applied at 16 grid points arranged in a 4×4 matrix (Fig. 1c), where the numbered #1-16 refers to the pulse numbers at grid points location. From the phase panel, it is evident that, upon applying fewer bias pulses, the purple-black ferroelectric domains ($P\downarrow$) are switched to yellow analogs ($P\uparrow$), with the polarization alignment with electric field direction ($E\uparrow P\uparrow$). Remarkably, as the pulses number increases, particularly after 13 pulses, the yellow domains ($P\uparrow$) can be switched to purple-black analogs ($P\downarrow$), with the polarization opposite to electric field direction ($E\uparrow P\downarrow$). The results clearly demonstrate the bidirectional domain switching under a unidirectional electric field. However, the topographical protrusions increase sharply as the polarization aligns oppositely to the electric field (Supplementary Fig. 1), suggesting that such anomalous polarization switching behavior is closely related to the enhanced Cu ion migration across the vdW gap. The surface bulge height reaches up to ~20 nm after 16 bias pulses. Currently, the direct atomic imaging of Cu ion migration coupled with polarization evolution via TEM faces fundamental obstacles in CIPS³⁷. However, EDX mappings demonstrate the long-range Cu ion migration across the vdW gap and the directionality of ion migration along the electric field^{38,39}.

Further, we fix the scanning tip location and apply 3 sets of bias (6 V for 5 s) at the central point location to manipulate the domain switching, as illustrated in Fig. 1d. After the 1st bias, the purple ferroelectric domains ($P\downarrow$) near the tip are switched to yellow analogs ($P\uparrow$). By continuously applying 2nd and 3rd bias pulses, the yellow domains ($P\uparrow$) can be reversibly switched back to purple-black analogs ($P\downarrow$). These results provide compelling evidence that the fixed unidirectional electric field enables the cyclic domain switching of $P\downarrow \rightarrow P\uparrow \rightarrow P\downarrow$. Such diverse polarization

configurations under electric field are the fundamental origin of multiple polarization states, such as quadruple and sextuple polarization states. However, the rapid formation of surface bulges (~35 nm) is a frustrating issue, as it means the irreversible damage to the material and hinders further ferroelectric domain manipulation in this target area.

Ion migration-mediated cyclic switching mechanism

By the switching spectroscopy PFM (SS-PFM)⁴⁰, the polarization switching dynamics under electric fields are further investigated. As shown in Fig. 2a, in a small window of $\pm 5 V_{dc}$, the phase shows one switching loop with -180° difference, and the amplitude presents two minima at the switching voltage, corresponding to the switching between two polarization states. The polarization aligns with the bias direction, and can be reversibly switched between $P\uparrow$ and $P\downarrow$ by applying an opposite bias direction. It is further revealed that two polarization states can be tunable into four or six states via electric field modulation. As the bias window extends, especially up to $\pm 13 V_{dc}$, both phase and amplitude exhibit three switching loops, corresponding to the order of six polarization states²¹. The phase can be switched six times by -180° , and the amplitude also shows six minima at each switching voltage (marked by black arrows). As positive bias ($E\downarrow$) increases, $P\uparrow$ is firstly switched to $P\downarrow$, then reversibly switched back to $P\uparrow$ with a cyclic switching of $P\uparrow \rightarrow P\downarrow \rightarrow P\uparrow$. Vice versa, a cyclic switching of $P\downarrow \rightarrow P\uparrow \rightarrow P\downarrow$ also occurs under the negative bias ($E\uparrow$). In this scenario, increasing the bias magnitude aligns the polarization opposite to the E -field direction ($E\uparrow P\downarrow$ or $E\downarrow P\uparrow$), mainly attributed to the Cu ions migration across the vdW gap²¹, which will be discussed in the following section. The repeated cycles further unveil the highly controllable Cu ion migration behaviors.

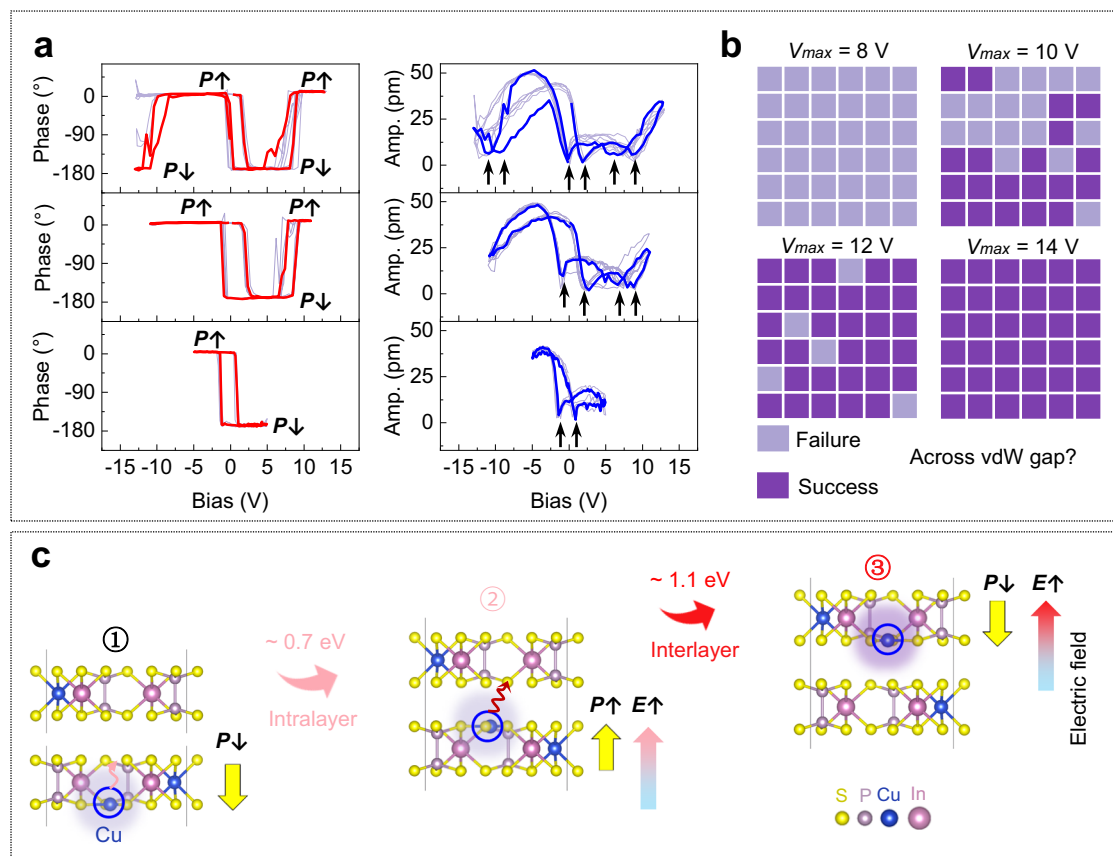


Fig. 2 | Ion migration-mediated domain switching mechanism. **a** The SS-PFM hysteresis loops measured at a fixed location by tuning the tip bias. **b** The statistical results of SS-PFM measured across 6×6 grid points location. **c** The schematic of Cu

ion migration pathways and polarization switching. Cu ion can migrate within the layer or across vdW gap dependent on the electric field with the migration barriers of ~ 0.7 and ~ 1.1 eV for intralayer and interlayer migration, respectively.

Additionally, Fig. 2b presents the statistical results of polarization switching loops measured across 6×6 grid points, and the detailed polarization switching curves are included in Supplementary Figs. 2–6. Here, we use the terms “Success” and “Failure” to describe whether Cu ions migrate across the vdW gap or not. Notably, the results indicate that a higher bias significantly increases the probability of mobile Cu ions across the vdW gap, thus aligning the polarization opposite to the E -field. Figure 2c further illustrates the Cu ion migration pathways and polarization switching. In our previous work⁴¹, the calculated barriers for the intralayer and interlayer Cu ions migration are -0.7 and -1.1 eV, respectively. The barrier deviation from switching voltage values for SS-PFM primarily arises from substantial tip-sample contact issues due to limited contact area (\sim nm scale), and easy degradation of the conductive tip coating during voltage application. However, the relative trend remains consistent, namely, the required voltage for intralayer migration is significantly lower than that for the interlayer migration. In

the case of low E -field or short time duration, the Cu ions can only hop up in the intralayer without the energy across the vdW gap, corresponding to the switching process from ① to ② state. In this scenario, the polarization aligns with the E -field direction. Once the E -field increases and/or the time duration extends, Cu ions can migrate across the vdW gaps into the adjacent layer with polarization opposite to E -field direction, as shown by the process from ② to ③ state.

Ferroelectric domain engineering with cyclic switching

To manipulate the domain switching over a large scale with minimal surface damage, another measurement setup has been utilized, as shown in Fig. 3a. Correspondingly, an insulating SiO_2/Si substrate is employed while bias voltage is applied through the tip. This setup establishes an electrically open-circuit condition without current generation. Compared to the closed-circuit setup, such an open-circuit setup effectively avoids the material damage from the tip-

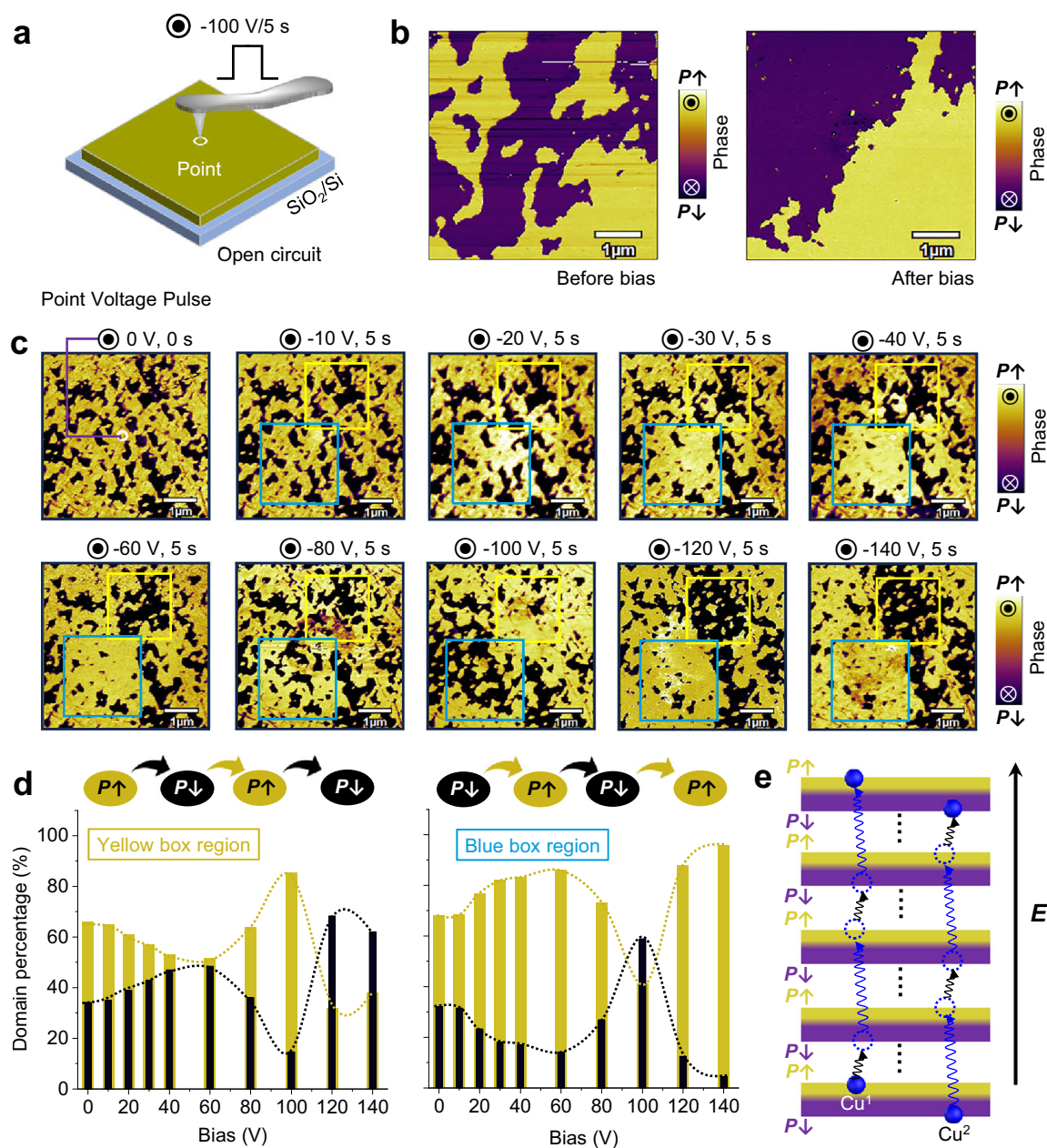


Fig. 3 | Cyclic and alternative switching of ferroelectric domains. a, b Schematic setup and bidirectional domain switching using a conductive tip. **c** The domain switching under a unidirectional electric field with progressively increased

magnitude. **d** Percentages of purple-black ($P \downarrow$) and yellow domains ($P \uparrow$) in the yellow- and blue- box regions. **e** Schematic Cu ions migration across the vdW layers for successive polarization switching.

concentrated current, favoring large-area ferroelectric domain manipulation and better switching stability (“Methods” and Supplementary Fig. 7). Moreover, Joule heating is also excluded as a contributing factor to the observed domain changes, since the tip-concentrated current is not involved. As shown in Fig. 3b, as -100 V ($\mathbf{E}\uparrow$) is applied for 5 s at the central point location, the switching scale of ferroelectric domains is remarkable up to $5\mu\text{m} \times 5\mu\text{m}$, which is ~ 4 orders of magnitude greater than the tip apex-CIPS contact area (tip apex radius: $\sim 25\text{ nm}$). While the charge modulation at the CIPS/substrate interface may influence polarization dynamics^{27,42}, the tip-induced microscale domain changes are primarily due to the inverted pyramidal geometry of the scanning tip (Supplementary Fig. 8). The switched domain area scales with the pyramid’s lateral dimensions, namely, larger sizes expand the switching regions, whereas small sizes confine the switching to smaller areas. The topographical data shows negligible surface damage, with protrusion heights of just $\sim 2\text{ nm}$ (Supplementary Fig. 9a).

In the top-left region, the yellow domains ($\mathbf{P}\uparrow$) are switched to purple-black analogs ($\mathbf{P}\downarrow$), with polarization opposite to the field direction ($\mathbf{E}\uparrow\mathbf{P}\downarrow$). Vice versa, in the bottom-right side, the purple-black domains ($\mathbf{P}\downarrow$) can be switched to yellow analogs ($\mathbf{P}\uparrow$), with polarization along the electric field direction ($\mathbf{E}\uparrow\mathbf{P}\uparrow$). These results confirm the reversible domains engineering at a large scale under unidirectional electric field. Interestingly, in the entire scanned region, the domain percentages of yellow ($\mathbf{P}\uparrow$) and purple-black domains ($\mathbf{P}\downarrow$) remain nearly unchanged, with a ratio close to 1:1 $\sim 51\%/49\%$ before the bias and $48\%/52\%$ after the bias, respectively. Moreover, these switched domains maintain their stability after the bias withdrawal (see Supplementary Fig. 9b).

Figure 3c investigates the domain switching behavior after applying the unidirectional bias ranging from -10 to -140 V ($\mathbf{E}\uparrow$) for 5 s in the central point location. Additional details on the surface topography, phase and amplitude before and after bias application are included in Supplementary Figs. 10, 11. Compared to surrounding regions, the domain changes are clearly visible within the yellow and blue boxes. The spatially selective switching responses are primarily attributed to the inhomogeneous field distribution applied by AFM tip approach (Supplementary Fig. 12). The two box regions are further selected to monitor the domain evolution. Correspondingly, the domain percentages of purple-black ($\mathbf{P}\downarrow$) and yellow domains ($\mathbf{P}\uparrow$), in response to various bias magnitudes in two selected regions are extracted, as presented in Fig. 3d. It discloses that, in yellow box region, the increased bias switches the ferroelectric domains in alternative sequence of $\mathbf{P}\uparrow \rightarrow \mathbf{P}\downarrow \rightarrow \mathbf{P}\uparrow \rightarrow \mathbf{P}\downarrow$, which includes two switching cycles of $\mathbf{P}\uparrow \rightarrow \mathbf{P}\downarrow \rightarrow \mathbf{P}\uparrow$ and $\mathbf{P}\downarrow \rightarrow \mathbf{P}\uparrow \rightarrow \mathbf{P}\downarrow$. Similarly, the blue box region also reveals an alternative switching of $\mathbf{P}\downarrow \rightarrow \mathbf{P}\uparrow \rightarrow \mathbf{P}\downarrow \rightarrow \mathbf{P}\uparrow$. Interestingly, the percentages of purple-black ($\mathbf{P}\downarrow$) and yellow domains ($\mathbf{P}\uparrow$) in the entire scanning region remain almost constant with the increase of bias magnitude (Supplementary Fig. 11b). The cyclic domain switching behavior can be highly reproducible (Supplementary Fig. 13), indicating the deterministic control. However, our conductive AFM-based experiments face some challenges. For instance, the conductive Pt/Ir tip coating deteriorates rapidly under repeated large voltage application, leading to the failure to achieve more switching cycles. While we cannot experimentally verify more at this stage, we believe that two key parameters, such as voltage magnitude and time duration, could affect the precise control of the switching cycles based on the field-dependent Cu ion migration.

Li et al.²¹ proposed a hybrid domain blocks (DBs) mechanism, where tip-induced E -field exponentially decayed with depth in CIPS flake and affected vertically stacked DBs that controlled the polarization states. However, our tomographic PFM (Supplementary Fig. 14) reveals uniform polarization configuration and consistent switching behavior throughout the entire CIPS nanoflake thickness, with no evidence of DBs. Accordingly, Fig. 3e further illustrates the scheme for

Cu ions migration and successive polarization switching. Assuming two Cu atoms (Cu^1 and Cu^2) initially occupy the upper/lower position within vdW layer, they generate $\mathbf{P}\uparrow/\mathbf{P}\downarrow$, respectively. With sustained large field application, Cu^1 and Cu^2 can progressively migrate across vdW layers to their accessible sites with successive polarization switching. More detailed discussions on the electric field-dependent Cu ions migration are illustrated in Supplementary Fig. 15. Additionally, we have fabricated few-layer (1-3 layers) CIPS on SiO_2/Si substrates via mechanical exfoliation, but no polarization switching is observed (Supplementary Fig. 16). Future investigations into polarization switching control in few-layer CIPS would be highly valuable, particularly to confirm monolayer-by-monolayer switching.

The “shape memory” effect during a cyclic switching

Through ultrafast scan imaging ($\sim 26\text{ s}$ per image) and repeated bias application, it is further revealed during a cyclic polarization switching that ferroelectric domains exhibit a remarkable “shape memory” effect, disappearing and reappearing with recoverable shape effect⁴³. The pristine ferroelectric domains are labeled as $\textcircled{1}$ state in Fig. 4a. We firstly apply -100 V ($\mathbf{E}\uparrow$) for 5 s at the central point location, then immediately withdraw the bias, and repeatedly scan to monitor the relaxation of the switched domains. Ultrafast scanning ($\sim 26\text{ s}$ per image) reveals a general phenomenon, namely, only a minor fraction of the switched domains rapidly relaxes within ~ 1 minute to their original shape upon large voltage withdrawal (Supplementary Fig. 17). However, under low voltage (-20 V for 10 s), the switched domains can be rapidly and fully recovered after field removal, and can reappear upon voltage reapplication (Supplementary Fig. 18). As shown in Fig. 4a, in the first 3 scans, a very short time of ~ 1 minute, only a small portion of switched domains are rapidly relaxed to their original shape, due to the imprint field from residual heterointerfaces charge or electrostatic potential^{38,44}. After 3rd scan, the switched domains retain good stability, consistent with the permanent retention reported for polarization written by an AFM tip³⁸. For example, in the purple box area, the yellow ferroelectric domains ($\mathbf{P}\uparrow$) are switched to purple-black analogs ($\mathbf{P}\downarrow$), and then remain stable over the time. The scans are extended to the 8th (corresponding to $\textcircled{3}$ state). Even after 3 h of voltage removal, the switched domains still remain stable (Supplementary Fig. 19). Therefore, the domain relaxation is not the primary cause of the subsequently observed domain shape memory effect. When -120 V ($\mathbf{E}\uparrow$) is further applied for 5 s, and then withdrawn, the purple-black domains ($\mathbf{P}\downarrow$) in the purple box area can be switched back to yellow analogs ($\mathbf{P}\uparrow$). In the entire process, the domains undergo a full cycle of $\mathbf{P}\uparrow \rightarrow \mathbf{P}\downarrow \rightarrow \mathbf{P}\uparrow$, and recover to their original polarization direction and domain shape, corresponding to the process from $\textcircled{1}$ to $\textcircled{3}$, and to $\textcircled{3}$ state (see more details in Supplementary Fig. 20). As far as we are aware, domain memory effect is rarely reported in conventional ferroelectrics, which not only indicates the highly controllable Cu ions migration, but also inspires the dynamic control for reservoir computing applications⁴⁵.

Figure 4b depicts the migration dynamics of Cu ions for cyclic polarization switching, which is critical for the observed domain memory effect. It is assumed that the Cu ion initially occupies the upper position of the vdW layer with upward polarization ($\mathbf{P}\uparrow$). Upon the 1st application of large electric field, the Cu ion migrates across the vdW layers to occupy the lower position with polarization switching ($\mathbf{P}\uparrow \rightarrow \mathbf{P}\downarrow$). Upon field withdrawal, merely a minor fraction of switched domains relaxes rapidly back to original state. However, the majority of switched domains retains good stability. With sustained electric field application, Cu ions can progressively migrate across vdW layers to occupy upper position of the neighbouring vdW layer with polarization switching ($\mathbf{P}\downarrow \rightarrow \mathbf{P}\uparrow$). Both the 1st and 2nd switching events observed in PFM imaging involve Cu migration across multiple layers, where both intralayer and interlayer migration keep happening. Two

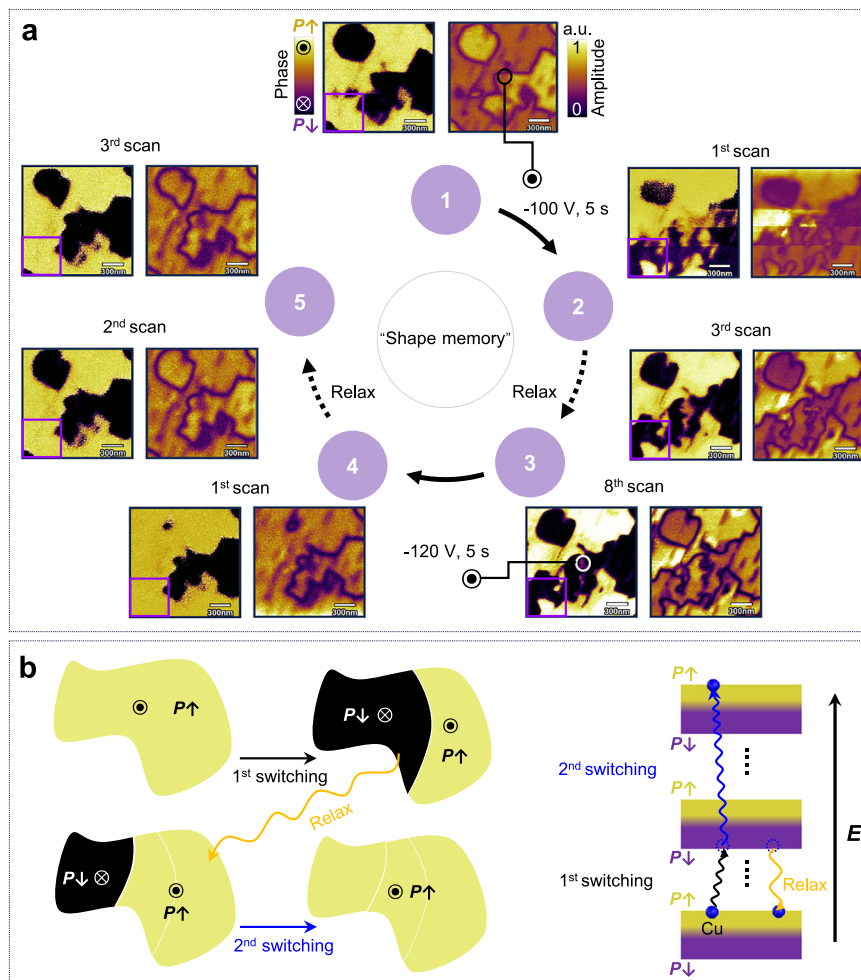


Fig. 4 | The “shape memory” behaviors of ferroelectric domains. a “Shape memory” effect of switched domains during a cyclic switching. In the purple box region, the ferroelectric domains exhibit a “shape memory” effect, disappearing

and reappearing with recoverable shape effect during a cyclic switching. **b** The schematic of cyclic domain switching behavior and successive Cu ions migration dynamics across the vdW layers.

successive events form a complete switching cycle ($P\uparrow \rightarrow P\downarrow \rightarrow P\downarrow$), during which Cu ions migrate upward by multiple vdW layers and restore the original polarization to enable the shape memory effect.

Electrically “writing” domain patterns

Finally, the unidirectional electric field is utilized to “write” a grid domain pattern with alternating $P\uparrow$ and $P\downarrow$ configurations. Figure 5a shows the bias map for electrically “writing” domains, under alternating -25 V ($E\uparrow$) and -50 V ($E\uparrow$) electric fields, as indicated by the red line profiles in Fig. 5b. The pristine domains prior to applied bias are shown in Fig. 5c, revealing the randomly distributed domain patterns. As demonstrated in Fig. 5d, the unidirectional bias can realize the precise control over the polarization directions ($P\uparrow$ and $P\downarrow$), and the well-defined grid patterns of ferroelectric domains are achieved under the given bias.

Figure 5e further shows the line profiles of given bias and the obtained domain configurations along the red line for multiple “writing” processes (see the details in Supplementary Fig. 21). It discloses that, in the -25 V ($E\uparrow$) poled region, the purple-black domains ($P\downarrow$) are switched to yellow analogs ($P\uparrow$), identical to the bias direction. Meanwhile, in the -50 V ($E\uparrow$) poled region, the yellow domains ($P\uparrow$) can be switched to purple-black analogs ($P\downarrow$), opposite to the bias direction. To the best of our knowledge, this is the first report of electrically “writing” ferroelectric domain patterns by a unidirectional electric field. The well-defined domain configurations in the 8×8 box

suggest the highly controllable electric field-driven Cu ions migration to different occupations, underscoring its potential for domain engineering and ferro-ionic device applications.

Discussion

Conventionally, ferroelectric materials usually require opposite (\pm) electric fields for reversible and cyclic ferroelectric domain switching. However, this scenario can be circumvented in vdW ferroelectrics CuInP_2S_6 , solely facilitated by a unidirectional electric field. This work unveils highly controllable Cu ion migration across vdW gap and confirms the effective domain engineering. For instance, the direction of polarization (P) can be alternatively switched by a unidirectional electric field following the sequence of $P\uparrow \rightarrow P\downarrow \rightarrow P\uparrow \rightarrow P\downarrow$, with two switching cycles $P\uparrow \rightarrow P\downarrow \rightarrow P\uparrow$ and $P\downarrow \rightarrow P\uparrow \rightarrow P\downarrow$. It further confirms the remarkable “domain shape memory effect” during cyclic switching, as well as the unprecedented ability to electrically “write” grid-patterned domain configurations enabled by the unidirectional field. These exotic ferroelectric domain dynamics stem from the vdW structure and bias-controlled ion migration across vdW gap. In principle, such phenomena should happen in all vdW ferroelectric systems sustaining such ionic motion. Crucially, these findings fundamentally advance our understanding of ferro-ionic coupling and provide critical insights into related exotic phenomena such as negative capacitance²², and quantized charge transport phenomena²⁸.

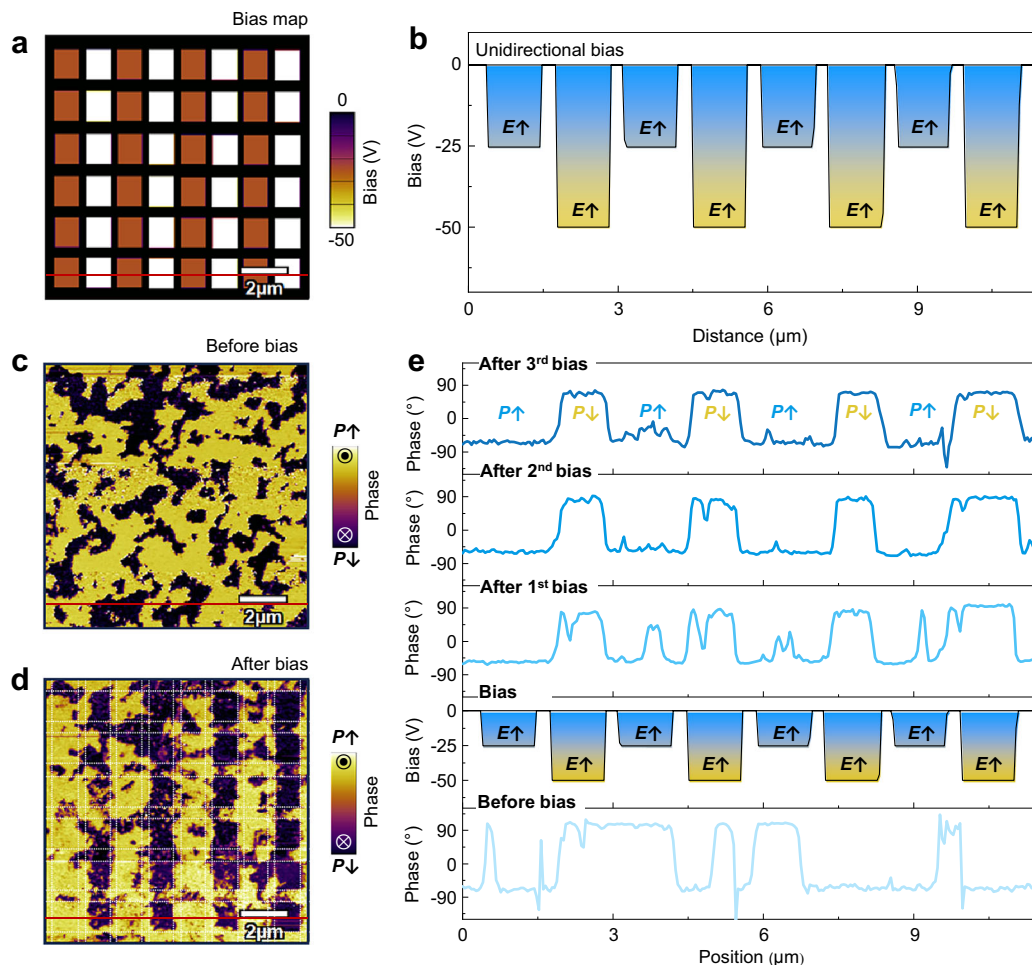


Fig. 5 | Electrical “writing” operation of ferroelectric domain configurations. **a** The unidirectional bias map for electrically “writing” grid-patterned ferroelectric domains. **b** The red line profiles of applied bias in (a). **c** Pristine domains with

randomly distributed domain patterns. **d** Grid-patterned ferroelectric domain arrangement after applying unidirectional bias. **e** The line profiles of applied bias and the domain arrangement along the red line for multiple “writing” processes.

Methods

Crystal growth and sample preparation

CIPS single crystals were synthesized using the chemical vapor transport (CVT) technique²⁵. In a typical process, the stoichiometric elemental precursors were placed in a vacuum-sealed quartz tube, maintained at a vacuum of -10^{-3} Pa. In the given two-zone tube furnace, the hot and cool zones were kept at -650 and -600 °C, respectively. The reaction was proceeded for -212 h. Thin CIPS flakes were obtained by mechanically exfoliating the CIPS crystal with the adhesive tape, subsequently transferred onto silicon substrates for subsequent PFM and SS-PFM characterizations.

Piezoresponse force microscopy measurement

Piezoresponse force microscopy (PFM) was measured on thin flakes using a commercial atomic force microscope (Cypher S, Oxford Instruments, USA), equipped with a high-voltage module. The vector PFM mode was used to image the ferroelectric domains by Pt/Ir-coated Si cantilever tip driven with an AC voltage of 1–2 V and with a frequency of -350 – 400 kHz. The hysteresis loops were measured using the Switching Spectroscopy PFM (SS-PFM) mode. Pulsed triangular DC voltage (V_{dc}) was used with a pulse width of 10 ms. A high-frequency AC voltage ($V_{ac} = 1$ V) was superimposed on the DC voltage. Multiple cycles of hysteresis loops were measured at a point location with the time duration of 1 s for each loop, consisting of 100 pulses. The off-field data were used for the analysis. To obtain the statistical results of bias-mediated polarization switching, SS-PFM

measurements were conducted across a 6×6 grid point location. In the litho-PFM, the time is fixed at 128 s per image in the litho-PFM mode for electrically “writing” grid-patterned domains. To investigate electric-field manipulation of ferroelectric domains, two different bias application methods were employed. One approach is to apply voltage through the bottom conductive substrate (Au/SiO₂/Si) under closed-circuit conditions, which easily caused significant surface damage and failed ferroelectric domain manipulation with domain switching only occurring in localized regions near the tip. In contrast, the alternative approach is to apply bias through a nanoscale tip under open-circuit conditions using an insulating SiO₂/Si substrate. This approach minimizes surface damage while achieving highly effective ferroelectric domain switching with a much larger switched domain area.

Simulation of electrostatic field distribution

The electrostatic field distribution between the nanometer tip and the ferroelectric CIPS sample was simulated by the finite element method. The CIPS nanosheet was set as a cylinder, and a spherical air domain was set on the periphery. The relative dielectric constants of air and CIPS are set to 1 and 40, respectively. The AC/DC physical field module was used, and the electrical boundary conditions were set. The bottom of CIPS was set to ground, which was regarded as the boundary potential of the spherical air domain at infinity, and a potential of set voltage was applied to the surface of the tip. The electrostatic field distribution was obtained by steady-state research.

Data availability

All data supporting the findings of this study are available within the article and the Supplementary Information file. Source data are provided with this paper.

References

- Kim, K. et al. Wurtzite and fluorite ferroelectric materials for electronic memory. *Nat. Nanotechnol.* **18**, 422–441 (2023).
- Yasuda, K. et al. Ultrafast high-endurance memory based on sliding ferroelectrics. *Science* **385**, 53–56 (2024).
- Sebastian, A. et al. Memory devices and applications for in-memory computing. *Nat. Nanotechnol.* **15**, 529–544 (2020).
- Wu, G. et al. Ferroelectric-defined reconfigurable homojunctions for in-memory sensing and computing. *Nat. Mater.* **22**, 1499–1506 (2023).
- Cui, B. et al. Ferroelectric photosensor network: an advanced hardware solution to real-time machine vision. *Nat. Commun.* **13**, 1707 (2022).
- Guo, M. et al. Toroidal polar topology in strained ferroelectric polymer. *Science* **371**, 1050–1056 (2021).
- Jiang, A. et al. Ferroelectric domain wall memory with embedded selector realized in LiNbO₃ single crystals integrated on Si wafers. *Nat. Mater.* **19**, 1188–1194 (2020).
- Si, M. et al. A ferroelectric semiconductor field-effect transistor. *Nat. Electron.* **2**, 580–586 (2019).
- Wu, J. et al. High tunnelling electroresistance in a ferroelectric van der Waals heterojunction via giant barrier height modulation. *Nat. Electron.* **3**, 466–472 (2020).
- Zhang, D. et al. Ferroelectric order in van der Waals layered materials. *Nat. Rev. Mater.* **8**, 25–40 (2023).
- Wang, C. et al. Towards two-dimensional van der Waals ferroelectrics. *Nat. Mater.* **22**, 542–552 (2023).
- Chang, K. et al. Discovery of robust in-plane ferroelectricity in atomic-thick SnTe. *Science* **353**, 274–278 (2016).
- Cui, C. et al. Intercorrelated in-plane and out-of-plane ferroelectricity in ultrathin two-dimensional layered semiconductor In₂Se₃. *Nano Lett.* **18**, 1253–1258 (2018).
- Yuan, S. et al. Room-temperature ferroelectricity in MoTe₂ down to the atomic monolayer limit. *Nat. Commun.* **10**, 1–6 (2019).
- Yasuda, K. et al. Stacking-engineered ferroelectricity in bilayer boron nitride. *Science* **372**, 1458–1462 (2021).
- Yang, X. et al. Highly reproducible van der Waals integration of two-dimensional electronics on the wafer scale. *Nat. Nanotechnol.* **18**, 471–478 (2023).
- Lu, D. et al. Monolithic three-dimensional tier-by-tier integration via van der Waals lamination. *Nature* **630**, 340–345 (2024).
- Liu, Y. et al. Van der Waals integration before and beyond two-dimensional materials. *Nature* **567**, 323–333 (2019).
- Martin, L. et al. Thin-film ferroelectric materials and their applications. *Nat. Rev. Mater.* **687**, 16087 (2016).
- Li, F. et al. Ultrahigh piezoelectricity in ferroelectric ceramics by design. *Nat. Mater.* **17**, 349–354 (2018).
- Li, T. et al. Realization of sextuple polarization states and interstate switching in antiferroelectric CuInP₂S₆. *Nat. Commun.* **15**, 2653 (2024).
- Neumayer, S. M. et al. The concept of negative capacitance in ionically conductive van der Waals ferroelectrics. *Adv. Energy Mater.* **10**, 2001726 (2020).
- Neumayer, S. M. et al. Alignment of polarization against an electric field in van der Waals ferroelectrics. *Phys. Rev. Appl.* **13**, 064063 (2020).
- Belianinov, A. et al. CuInP₂S₆ room temperature layered ferroelectric. *Nano Lett.* **15**, 3808–3814 (2015).
- Liu, F. et al. Room-temperature ferroelectricity in CuInP₂S₆ ultrathin flakes. *Nat. Commun.* **7**, 12357 (2016).
- Brehm, J. A. et al. Tunable quadruple-well ferroelectric van der Waals crystals. *Nat. Mater.* **19**, 43–48 (2020).
- Wang, K. et al. Interface-tuning of ferroelectricity and quadruple-well state in CuInP₂S₆ via ferroelectric oxide. *ACS Nano* **17**, 15787–15795 (2023).
- Seleznev, D. et al. Cyclic ferroelectric switching and quantized charge transport in CuInP₂S₆. *Phys. Rev. B* **108**, L180101 (2023).
- Wang, X. et al. Unconventional ferroelectricity with quantized polarizations in ionic conductors: high-throughput screening. *J. Phys. Chem. Lett.* **13**, 9552–9557 (2022).
- Chen, M. et al. Selective and quasi-continuous switching of ferroelectric Chern insulator devices for neuromorphic computing. *Nat. Nanotechnol.* **19**, 962–969 (2024).
- Ming, W. et al. Flexoelectric engineering of van der Waals ferroelectric CuInP₂S₆. *Sci. Adv.* **8**, eabq1232 (2022).
- Balke, N. et al. Locally controlled Cu-ion transport in layered ferroelectric CuInP₂S₆. *ACS Appl. Mater. Interfaces* **10**, 27188–27194 (2018).
- Zhu, H. et al. Highly tunable lateral homojunction formed in two-dimensional layered CuInP₂S₆ via in-plane ionic migration. *ACS Nano* **17**, 1239–1246 (2023).
- Zhou, J. et al. 2D ferroionics: conductive switching mechanisms and transition boundaries in van der Waals layered material CuInP₂S₆. *Adv. Mater.* **35**, 2370267 (2023).
- Dawei, Z. et al. Anisotropic ion migration and electronic conduction in van der Waals ferroelectric CuInP₂S₆. *Nano Lett.* **21**, 995–1002 (2021).
- Zhong, Z. et al. Robust threshold-switching behavior assisted by Cu migration in a ferroionic CuInP₂S₆ heterostructure. *ACS Nano* **17**, 12563–12572 (2023).
- Guo, C. et al. Atomic-level direct imaging for Cu (I) multiple occupations and migration in 2D ferroelectric CuInP₂S₆. *Nat. Commun.* **15**, 10152 (2024).
- Zhou, S. et al. Anomalous polarization switching and permanent retention in a ferroelectric ionic conductor. *Mater. Horiz.* **7**, 263–274 (2020).
- Zhong, Z. et al. Reconfigurable logic circuits and rectifier based on two-terminal ionic homojunctions. *Device* **3**, 12563–12572 (2025).
- Jesse, S. et al. Switching spectroscopy piezoresponse force Microscopy of ferroelectric materials. *Appl. Phys. Lett.* **88**, 062908 (2006).
- Jiang, X. et al. Dual-role ion dynamics in ferroionic CuInP₂S₆: revealing the transition from ferroelectric to ionic switching mechanisms. *Nat. Commun.* **15**, 10822 (2024).
- Hou, X. et al. Optical evidence of interfacial strain-induced ferroelectric tuning and enhancement in CuInP₂S₆ via ferroelectric substrate. *Small* **21**, 2409879 (2025).
- Wang, Z. et al. Domain memory effect in the organic ferroics. *Nat. Commun.* **13**, 2379 (2022).
- Lee, D. et al. Active control of ferroelectric switching using defect-dipole engineering. *Adv. Mater.* **24**, 6490 (2012).
- Everschor-Sitte, K. et al. Topological magnetic and ferroelectric systems for reservoir computing. *Nat. Rev. Phys.* **6**, 455–462 (2024).

Acknowledgements

We acknowledge Prof. Ruirui Niu for the preparation of few-layer nanoflakes and Prof. Ruizhi Yu for helpful discussion. This work is supported by the Ningbo Yongjiang Talent Introduction Program No. 2023A-390-G (X. J.) and Ningbo Top Talent Project No. 2020-DST-003 (W. Y.), the National Natural Science Foundation of China Nos. 12374080 (X. Y. W.), 12202056 (X. J.), 52372063 (W. Y.), 92163101 (X. Y. W.), 12474101 (X. L. W.), 12304120 (J. D.).

Author contributions

Z. L., X. Y. W. and W. Y. conceived the idea and directed the project. Y. C. and J. D. provided the single-crystal sample. X. J. performed the PFM measurements. M. L. gave the assistance with data collection. X. J., Z. L., X. Y. W. and W. Y. carried out the data analyses and cowrote the manuscript. X. Z. provided the tip-electric field calculation. X. W., Z. D., X. L. W., D. Z., X. Y., Z. P. contributed to the discussion.

Competing interests

The authors declare no competing interests.

Additional information

Supplementary information The online version contains supplementary material available at <https://doi.org/10.1038/s41467-025-63049-2>.

Correspondence and requests for materials should be addressed to Zhao Liang, Xueyun Wang or Weiyu Yang.

Peer review information *Nature Communications* thanks Yi-De Liou, and the other anonymous reviewer(s) for their contribution to the peer review of this work. A peer review file is available.

Reprints and permissions information is available at <http://www.nature.com/reprints>

Publisher's note Springer Nature remains neutral with regard to jurisdictional claims in published maps and institutional affiliations.

Open Access This article is licensed under a Creative Commons Attribution-NonCommercial-NoDerivatives 4.0 International License, which permits any non-commercial use, sharing, distribution and reproduction in any medium or format, as long as you give appropriate credit to the original author(s) and the source, provide a link to the Creative Commons licence, and indicate if you modified the licensed material. You do not have permission under this licence to share adapted material derived from this article or parts of it. The images or other third party material in this article are included in the article's Creative Commons licence, unless indicated otherwise in a credit line to the material. If material is not included in the article's Creative Commons licence and your intended use is not permitted by statutory regulation or exceeds the permitted use, you will need to obtain permission directly from the copyright holder. To view a copy of this licence, visit <http://creativecommons.org/licenses/by-nc-nd/4.0/>.

© The Author(s) 2025